



OPEN

Electric field tuning of a nickel zinc ferrite resonator by non-linear magnetoelectric effects

Maksym Popov^{1,2}, Alexander Machi², Jerad Inman³, Rao Bidthanapally², Sujoy Saha², Hongwei Qu³, Menka Jain⁴, Michael R. Page⁵ & Gopalan Srinivasan²✉

The nature of nonlinear magnetoelectric (NLME) effect has been investigated at room-temperature in a single-crystal Zn substituted nickel ferrite. Tuning of the frequency of magnetostatic surface wave (MSSW) modes under an applied pulsed DC electric field/current has been utilized to probe the effect. The frequencies of the modes at 8–20 GHz were found to decrease by ~ 400 MHz for an applied DC power P of ~ 100 mW and the frequency shift was the same for all of the MSSW modes and linearly proportional to P . A model is proposed for the effect and the NLME phenomenon was interpreted in terms of a reduction in the saturation magnetization due to the DC current. The decrease of magnetization with applied electric power, estimated from data on mode frequency versus P , was ~ 2.50 G/mW. The frequency tuning efficiency of the MSSW modes due to NLME effects in the ferrite resonator was found to be 4.1 MHz/mW which is an order of magnitude higher than the shift reported for M-type strontium and barium hexaferrite resonators investigated earlier. The spinel ferrite resonator discussed here has the potential for miniature, electric field tunable, planar microwave devices for the 8–20 GHz frequency range.

Microwave devices such as resonators and band-stop and band-pass filters are important components in high frequency communication devices and radars^{1–3}. Such devices, in general, are based on low-loss semiconductors, ferroelectrics, or ferrites^{1–6}. Tuning the operating frequencies of ferroelectric devices could be accomplished with an electric field E and the devices could easily be miniaturized. The frequency of ferrite-based devices, however, could only be tuned with a source of variable magnetic field H ^{4–8}. Thus, ferrite microwave devices cannot be miniaturized or integrated with semiconductor devices due to the need for a solenoid or similar sources to generate a variable H . A significant development in microwave device technologies is the use of a ferrite-ferroelectric composite to facilitate E tuning of the ferrite devices^{9–12}. The E -tuning is possible due to magneto-electric (ME) effect in such composites^{13, 14}. The piezoelectric strain under an E -field in the composite when transferred to the ferrite manifests as an induced magnetic field and leads to tuning of the ferrite device^{12–15}. A variety of dual H - and E -tunable ferrite-ferroelectric devices including resonators, filters, and inductors were demonstrated in the past years^{16–20}.

An alternate E -tuning mechanism of ferrite devices aided by non-linear ME effect (NLME) was reported recently^{21, 22}. The NLME effect, first reported in M-type strontium hexagonal ferrite, was observed as tuning of ferromagnetic resonance (FMR) in the ferrite under a DC or pulsed E -field. The E/I -induced changes in the magnetization and anisotropy field due to NLME, determined from FMR data, were found to vary with the input DC power (or E^2). Studies on c -plane single crystals of (Sr, Al)- and Ba-hexaferrites also revealed a similar NLME effects for currents either in the c -plane or along the c -axis^{23, 24}. E -tunable resonators and filters of M- and Y-type hexagonal ferrites operating at 12–50 GHz were demonstrated^{25–27}.

This report is on the first observation of a similar NLME effect in a spinel ferrite with cubic symmetry. We present here experimental evidence for the effect in a microwave resonator with a single crystal platelet of nickel zinc ferrite. The device operates in the X- to K-bands, thus complements similar resonators and filters that make use of hexaferrites for higher frequencies. Besides, nickel ferrite easily adopts to dopants such as Zn which makes possible tuning of its magnetic parameters for ferrite devices operating at a specific frequency range²⁸. The experiments were carried out with the ferrite in a stripline device structure and a static magnetic field H_0 was

¹Institute of High Technologies, Taras Shevchenko National University of Kyiv, Kyiv 01601, Ukraine. ²Department of Physics, Oakland University, Rochester, MI 48309, USA. ³Electrical and Computer Engineering Department, Oakland University, Rochester, MI 48309, USA. ⁴Department of Physics, University of Connecticut, Storrs, CT 06269, USA. ⁵Materials and Manufacturing Directorate, Air Force Research Laboratory, Wright-Patterson Air Force Base, Dayton, OH 45433, USA. ✉email: srinivas@oakland.edu

applied to excite magnetostatic surface wave (MSSW) modes in the 8–20 GHz frequency range^{29,30}. An in-plane DC current applied parallel to H_0 resulted in a down shift in the mode frequencies of equal magnitude for all of the modes. The decrease in the mode frequency Δf was in excess of 400 MHz for a DC power $P \sim 400$ mW and Δf was found to vary linearly with P . Data on mode frequency f versus P was used to estimate the changes in the magnetic parameters for the ferrite. Since the frequency shift due to NLME effects is similar to the influence of sample heating, experiments carried out to determine the Joule heating effect indicated a frequency shift that was an order of magnitude smaller than the shift due to NLME effects. Details on our studies are provided in the sections that follow.

Experiment

The material under investigation was a single-crystal platelet of zinc-substituted nickel ferrite with the composition $\text{Ni}_{0.7}\text{Zn}_{0.3}\text{Fe}_2\text{O}_4$ (NZFO) grown by floating zone technique (and provided by Professor A. Balbashov, Moscow Power Engineering Institute, Russia). It was cut into rectangular slabs in such way that the crystallographic $\langle 111 \rangle$ direction coincided with the normal to the sample plane. It was then polished down to a thickness of $S = 335$ μm and to the lateral dimensions $a \times b = 2.5 \times 1$ mm^2 . Finally, conducting electrodes (3 μm of Pt on 45 nm Ti buffer layer) as shown in Fig. 1 were deposited on opposite sides of samples by magnetron sputtering. Those electrodes provided a path for current flow through the NZFO in the (111) plane along the longer side. Figure 1 shows the experimental setup with the NZFO sample placed on top of a microstrip transmission line. The current I is parallel to the static field H_0 , along the Z -direction. The sample is separated from the stripline by an adhesive dielectric layer of thickness D_1 .

Since the DC electric field/current is a key parameter in the measurements, the voltage V versus current I characteristics were measured for the sample and are shown in Fig. 2. The current I varies linearly with V for $V < 2$ V, corresponding to a resistance $R \sim 510$ Ω , and a nonlinear variation in I is evident for higher V values.

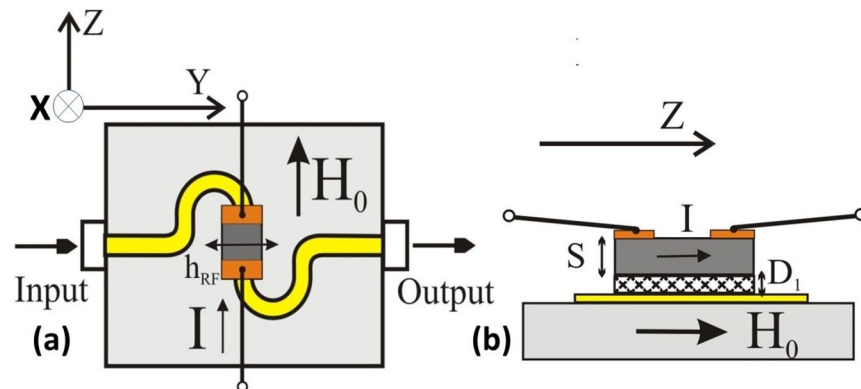


Figure 1. (a) Schematic diagram showing the experimental setup with the nickel zinc ferrite sample, $\text{Ni}_{0.7}\text{Zn}_{0.3}\text{Fe}_2\text{O}_4$ (NZFO), with Pt-electrodes placed on top of a microstrip line. (b) Cross section view of the NZFO samples. S is the sample thickness and D_1 is the thickness of an adhesive epoxy layer. The static field H_0 and the DC current I are applied along the Z -direction.

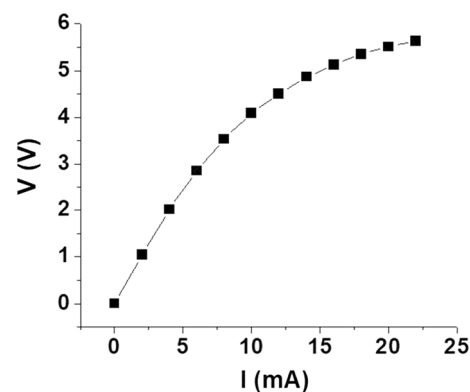


Figure 2. DC voltage V versus current I data for the NZFO sample.

Results

The NZFO sample was placed on top of a S-shaped microstrip line etched on a 0.02 inch (508 μm) thick RT/Duroid 5880 substrate. A thin adhesive tape of thickness of thickness $D_1 = 20 \mu\text{m}$ was used to fix the sample in place. A bias magnetic field H_0 was applied along the longer side of the sample for the excitation of MSSW modes in the ferrite. The stripline structure with the NZFO sample was connected to the ports of a vector network analyzer (Agilent PNA E8361A) and excited with microwave power (Figure S-1). The scattering matrix parameter S_{21} for the resonator was measured as a function of the frequency f of the input microwave power. Representative S_{21} versus f profiles for $H = 665 \text{ Oe}$ and 2725 Oe are shown in Fig. 3. Depending on H_0 values, several MSSW modes were observed in the frequency range 8–16 GHz. The two dominant modes are shown in Fig. 3. Similar measurements were done for a series of H_0 values ranging from 400 to 4400 Oe (corresponding to $f_r \approx 8$ –20 GHz) (Figure S-2). Data on the variation of f_r with H obtained from such profiles are shown in Fig. 4 (and also in Figure S-3).

Following the measurements of f_r versus H_0 , studies were carried out on the tuning of the resonator mode frequency with a DC E/I for constant H_0 values. A DC voltage single pulse, 1–5 s in duration, applied to the electrodes (shown in Fig. 1), established a current parallel to H_0 . Successive pulses were applied after a time interval of 1 min to minimize potential heating of the sample. Figure 5 shows a series of S_{21} versus f profiles for the two dominant MSSW modes for H_0 value of 2045 Oe and $I = 0$ –20 mA. The E/I -induced shift in the mode frequency Δf_r is also shown for the two modes as a function of the input power P . It is clear from the results that Δf_r for the two modes are approximately the same for a specific P -value. Both modes show a decrease in the frequency shift with increasing input power and their dependence on P is linear. Similar linear variation in Δf_r was measured for a series of bias magnetic fields as shown in Fig.S-4–S-7 in the supplement. From now on we, therefore, focus only on results obtained for the higher frequency MSSW mode.

Results on the I -tuning of the high frequency mode are shown in Fig. 6 for $H_0 = 1355 \text{ Oe}$ and 3440 Oe and the variation in the mode frequency shift Δf_r with P is shown in Fig. 7 for a series of H_0 values. It is evident that the measured decrease in Δf_r with P is independent for H_0 value. It is also obvious from the data in Fig. 7 that the E -tuning of the mode frequency is due to nonlinear ME effects and Δf_r is proportional to E^2 (and not just E).

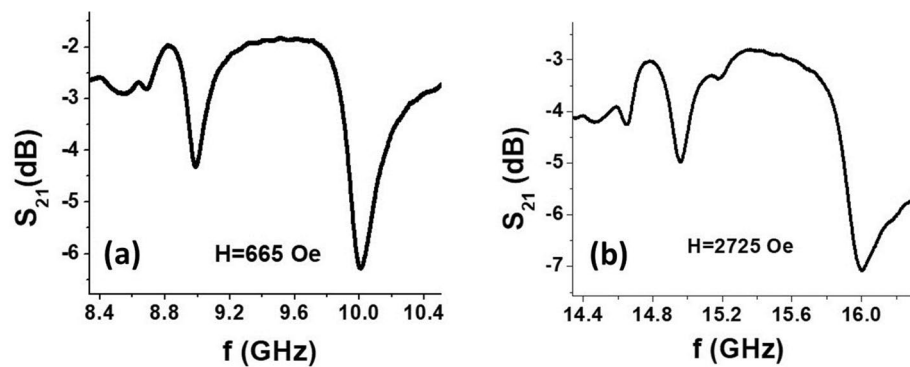


Figure 3. Transmission loss S_{21} as a function of frequency f for NZFO sample for an in-plane static magnetic field (a) $H = 665 \text{ Oe}$ and (b) 2725 Oe . The profiles show two dominant magnetostatic surface wave (MSSW) modes.

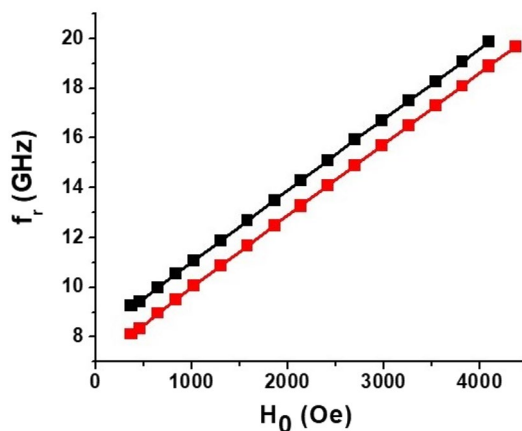


Figure 4. MSSW mode frequency f_r as a function of the applied magnetic field H_0 for the two dominant modes as in Fig. 3.

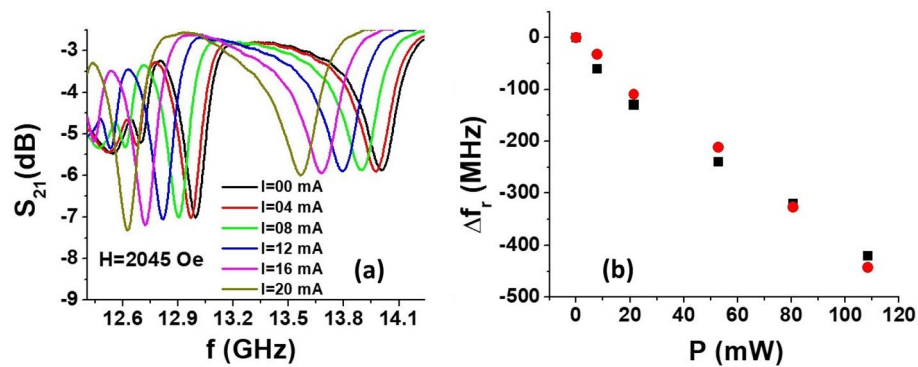


Figure 5. (a) Profiles of S_{21} versus f showing the current tuning of the dominant resonance modes in the NZFO platelet for $H = 2045$ Oe for $I = 0$ –20 mA. (b) Variation in the I -induced shift Δf_1 in the lower (squares) and higher (circles) frequency modes with the input DC power P .

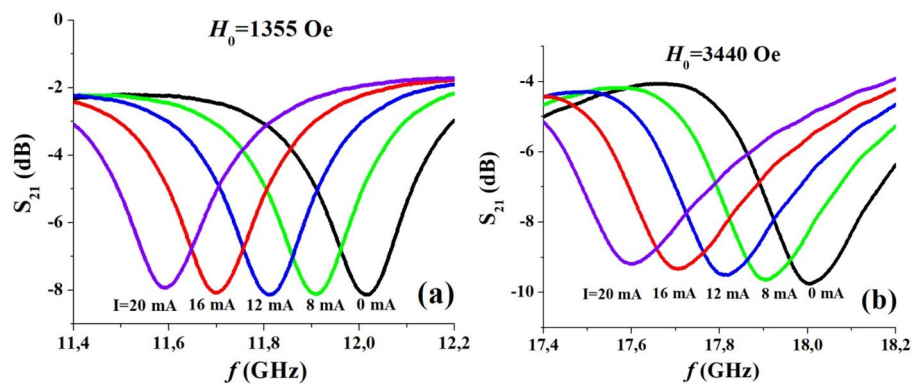


Figure 6. Representative data for current tuning of the high frequency MSSW modes in (111) NZFO resonator for the current flowing parallel to in-plane magnetic field H_0 .

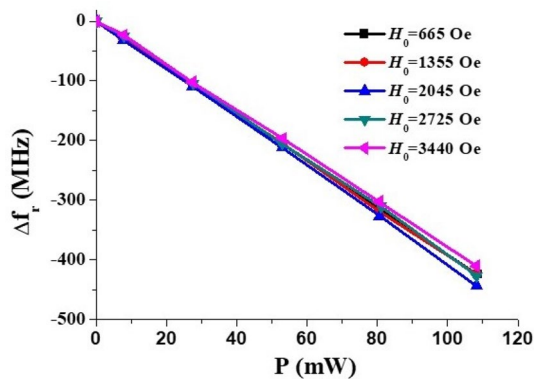


Figure 7. Shift in the MSSW mode frequency versus applied electric power measured for a series of magnetic bias field values.

The data also allows one to extract the efficiency of tuning, the slope $\Delta f_1/\Delta P$, for meaningful comparison with other materials or electrically tunable ferrite devices. The tuning efficiency is $\Delta f_1/\Delta P \sim 4.1$ MHz/mW for the NZFO resonator. Comparison of the tuning efficiency with similar ferrite devices are provided in later sections.

Discussion

Linear ME effects mediated by mechanical deformation have been studied extensively in composites of ferrites and ferroelectrics^{12–14}. Due to symmetry considerations such linear ME effects, however, are forbidden in ferrites with collinear magnetic ordering. A theory for the NLME effects observed in both hexagonal^{21–27} and

spinel ferrites is lacking at present. One may attribute the NLME to weakening of the magnetic interactions due to the exclusion of electrons involved in carrying a current in the ferrite under a DC electric field. Even though stoichiometric spinel ferrites are expected to be insulators, divalent Fe are generally present in them due to impurities. Hopping type conduction in the ferrites, therefore, leads to a semiconductor like behavior. Under an applied DC voltage, electrons in Fe sites involved in carrying a current are likely to be excluded from contributing to super-exchange interactions. Weakening of the magnetic interactions will lead to a decrease in the overall magnetization of the ferrite. That exclusion will be in effect for during the time electrons hop from one iron site to another. One may, therefore, attribute the decrease in the magnetization that manifests as a decrease in the frequency of resonance modes to weakening of magnetic exchange interactions and consequent decrease in the magnetization.

We first discuss a model for the MSSW modes and their E -tuning in a uniformly magnetized ferrite platelet enclosed between conducting metal layers, with ferrite to metal spacings equal to D_1 and D_2 ³⁰. The explicit dispersion equation for this case is given by Eq. (6) in Ref.³⁰ which is:

$$(1 + \kappa)(1 + \kappa + \eta^2) - \left(v - \sqrt{1 + \eta^2} \tanh \left(\frac{D_1}{S} \varsigma \sqrt{1 + \eta^2} \right) \right) \left(v + \sqrt{1 + \eta^2} \tanh \left(\frac{D_2}{S} \varsigma \sqrt{1 + \eta^2} \right) \right) + (1 + \kappa) \sqrt{1 + \eta^2} \sqrt{1 + \frac{\eta^2}{1 + \kappa}} \left(\tanh \left(\frac{D_1}{S} \varsigma \sqrt{1 + \eta^2} \right) + \tanh \left(\frac{D_2}{S} \varsigma \sqrt{1 + \eta^2} \right) \right) \coth \left(\varsigma \sqrt{1 + \frac{\eta^2}{1 + \kappa}} \right) = 0 \quad (1)$$

where $\kappa = \Omega_H / (\Omega_H^2 - \Omega^2)$, $v = \Omega / (\Omega_H^2 - \Omega^2)$, $\Omega_H = H_0 / (4\pi M_0)$, $\Omega = \omega / (\gamma 4\pi M_0)$, $\xi = k_z S$, $\zeta = k_y S$, and $\eta = \xi / \zeta = k_z / k_y$. Here $4\pi M_0$ is the saturation magnetization of the ferrite, $\gamma = 2.8$ MHz/Oe²⁸ is the gyromagnetic ratio. The coordinate system used here is shown on the Fig. 1.

In our experimental set-up the bottom metal layer is the central stripe of the S-shaped microstrip line (Fig. 1) of width same as the resonator width b . The distance between the bottom metal layer and the ferrite is $20 \mu\text{m}$ which is the thickness of the adhesive layer. The top metal layer is formed by the Pt electrodes that partially cover the sample surface. In essence, the ferrite sample consists of two regions with different MSSW dispersion characteristics $\omega(k)$. The first one is the middle area with only the bottom metal screen. The dispersion equation for this region can be obtained from Eq. (1) by substituting the screen spacing $D_1 = 20 \mu\text{m}$ and $D_2 = \infty$, respectively:

$$(1 + \kappa)(1 + \kappa + \eta^2) - (v - \text{sgn}(\varsigma) \sqrt{1 + \eta^2}) \left(v + \sqrt{1 + \eta^2} \tanh \left(\frac{D_2}{S} \varsigma \sqrt{1 + \eta^2} \right) \right) + (1 + \kappa) \sqrt{1 + \eta^2} \sqrt{1 + \frac{\eta^2}{1 + \kappa}} \left(\text{sgn}(\varsigma) + \tanh \left(\frac{D_2}{S} \varsigma \sqrt{1 + \eta^2} \right) \right) \coth \left(\varsigma \sqrt{1 + \frac{\eta^2}{1 + \kappa}} \right) = 0 \quad (2)$$

The second region is the ferrite under the Pt electrodes. This case is described by conditions $D_1 = 20 \mu\text{m}$ and $D_2 = 0$, which leads to the following dispersion equation^{29,30}

$$(1 + \kappa)(1 + \kappa + \eta^2) - v \left(v + \sqrt{1 + \eta^2} \tanh \left(\frac{D_2}{S} \varsigma \sqrt{1 + \eta^2} \right) \right) + (1 + \kappa) \sqrt{1 + \eta^2} \sqrt{1 + \frac{\eta^2}{1 + \kappa}} \tanh \left(\frac{D_2}{S} \varsigma \sqrt{1 + \eta^2} \right) \coth \left(\varsigma \sqrt{1 + \frac{\eta^2}{1 + \kappa}} \right) = 0 \quad (3)$$

[all the notations are the same as in Eq. (1)]. The above equations are valid for an isotropic ferromagnet and thus can be applied in practice only in the situation when the anisotropy field is negligible in comparison to both the static magnetization and H_0 which is true for the NZFO used in this study²⁸. The presence of the metal screen leads to a pronounced nonreciprocity of the MSSW propagation, namely, the waves with the opposite directions of the wave-vector will have different frequencies: $\omega(k) \neq \omega(-k)$. That fact strongly influences the resonator modes since they are usually formed by the interference of the counter-propagating waves. An example for the nonreciprocal dispersion characteristics of the MSSW in both regions of the resonator is shown in the Fig. 8.

In order to determine the resonance frequencies of the ferrite one needs to define the in-plane wave-vector set by the geometric dimensions of the resonator. The sign of longitudinal wave-vector k_z (or ξ) (with respect to the H_0 direction) does not affect the dispersion Eqs. (2) or (3) and therefore it can be calculated as

$$k_z = m \frac{\pi}{d}, m = 0, 1, 2, \dots \quad (4a)$$

Here d is the length of the metal electrode ($d \approx 0.7$ mm in our case) or the distance of metal-free region between the electrodes. On the other hand, the transversal wave-vector k_y due to the nonreciprocity of MSSW should be evaluated from the condition³¹

$$(k_y^+ + |k_y^-|)b = 2\pi n, n = 0, 1, 2, \dots \quad (4b)$$

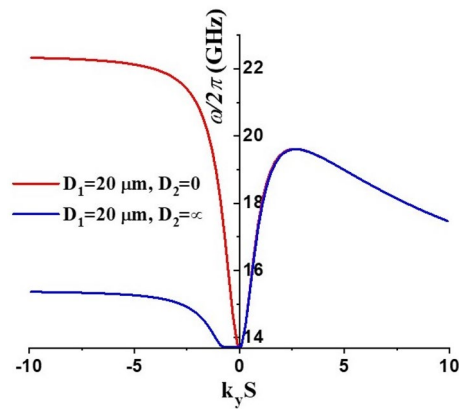


Figure 8. Nonreciprocal dispersion characteristic of MSSW in an isotropic ferrite layer calculated using Eqs. (1) and (2) and for $H_0 = 3000$ Oe, $4\pi M_0 = 5000$ G and $\xi = 1$. Note, that for the positive values of wavevector ($k_y > 0$) the dispersion curves for $D_2 = 0$ and $D_2 = \infty$ are nearly identical (frequency difference is less than 150 MHz for the given parameters).

where k^\pm are the positive and negative solutions of the Eq. (2) or (3) and b is the width of the sample. The modes represented by Eqs. (4a) and (4b) will therefore be labeled as (m, n) modes. The observed FMR frequency variation is given by

$$\Delta f_r = \frac{\partial f_r}{\partial (4\pi M_0)} \Delta(4\pi M_0) \quad (5)$$

Assuming that $\Delta(4\pi M_0)$ is linearly proportional to the applied power^{21–24}, the expected shift Δf_r also should be proportional to P which agrees with the results in Fig. 7. One may then use the above theory to extract the NLME induced variation in the saturation magnetization. For the nickel-zinc ferrite of the given composition $4\pi M_0 \approx 5000$ G whereas the cubic anisotropy field H_a is less than 100 Oe²⁸. Therefore, the condition $4\pi M_0 > H_a$ is fulfilled and use of Eqs. (2), (3) is justified.

The higher frequency mode shown in Fig. 3 was identified as (1, 1) mode of the metalized ferrite region. We used this mode to estimate the NLME induced changes in magnetization from Δf_r versus P data in Fig. 7. The following procedure was used for the estimate. For specific f_r and $4\pi M_0 \approx 5000$ G, $\gamma = 2.8$ MHz/Oe, and the dimensions of the resonator (d, b, S) the wave-vector values k^\pm were calculated from Eq. (2). Then the values of k^\pm were substituted into Eq. (4b) and checked whether this equation was satisfied. If not, then the procedure was repeated for series of values of $4\pi M_0$ until the wave vector values satisfied both Eq. (3) and Eq. (4b). This procedure was repeated for f_r corresponding to different values of P to determine the variation of $4\pi M_0$ with P . The results on $4\pi M_0$ versus P for a series of H_0 values are shown in Fig. 8. We took only the data for the largest values of external bias field since in this case the influence of static demagnetization field (that was not taken into account in Eq. (1)–(3)) is expected to be minimal. One notices a linear decrease in $4\pi M_0$ at an average rate of $-(2.50 \pm 0.12)$ G/mW for all of the H_0 values. The deviation in $4\pi M_0$ at $P = 0$ from the expected value of 5000 G may be attributed to the contribution from the cubic anisotropy field $H_a \sim 100$ Oe²⁹. Additionally, one may expect a variation in the cubic anisotropy field on E ³² due to NLME effects which was not considered in the model discussed here.

In the course of the measurements the DC voltage/current was applied as short pulses to the nickel ferrite sample in order to eliminate the effect of Joule heating of the sample and its contribution to any changes in f_r . The pulses were of duration 1–5 s. It is important to investigate the effects of sample heating compared to the influence of NLME effects. Additional experiments were done to separate these two effects on the decrease in the mode frequency under a DC current. Although the data provided in Figs. 3, 4, 5, 6, 7 and 9 (in the revised version) are for pulsed currents of duration 1–5 s, we examined the effects of sample heating under a *continuous DC current*. The current, corresponding to input power $P = 55$ mW and 103 mW, was first turned on for a duration of 10 min and the resonance frequency f_r was recorded at regular time intervals. The current was then turned off after 10 min, and data on f_r versus t were recorded for the next 10 min. The results on Δf_r versus t are shown in Fig. 10. For both DC powers, Δf_r shows an abrupt decrease by 180 MHz for $P = 55$ mW and by 410 MHz for $P = 103$ mW as soon as the current is on and then shows a further decrease by 5–15 MHz over the 10 min period that the current was present. As soon as the current is turned off, f_r shows an abrupt increase and Δf_r slowly decays to zero during the next 10 min of cooling. It is therefore evident from these experiments that Joule heating results only in 4–8% of the overall shift due to NLME effects.

The ferrite platelet in our experiments had a large surface area-to-volume ratio that is favorable in terms of effective heat exchange. The top surface was exposed to air and the bottom surface with a thin adhesive layer is on top of the thermally conducting copper microstrip line. If the sample were thermally isolated and under a prolonged application of a continuous DC current, the temperature (and thus mode frequency) should continuously change with time. But data in Fig. 10 shows that this is not the case. Next, such thermally isolated sample

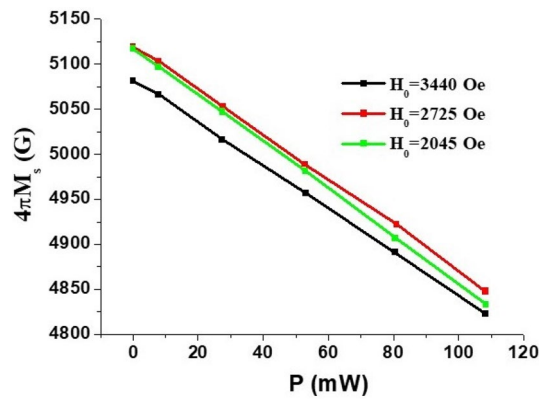


Figure 9. Calculated dependence of the nickel-zinc ferrite saturation magnetization $4\pi M_0$ on the applied dc electric power P .

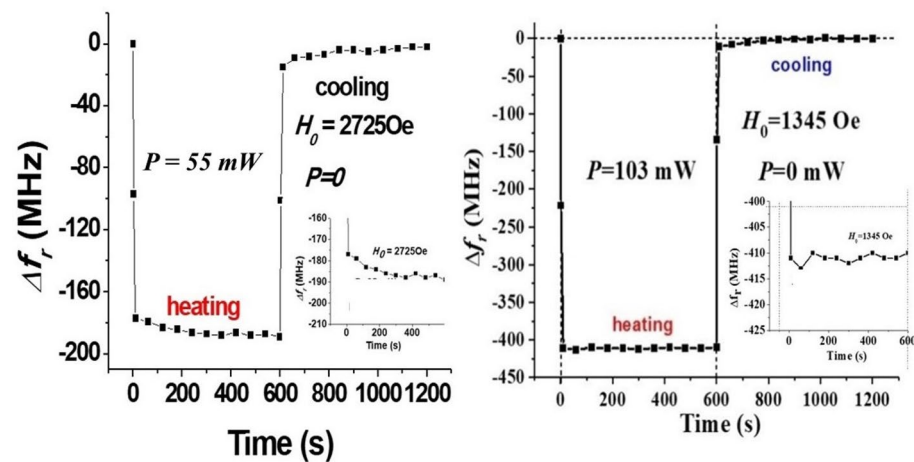


Figure 10. Data on Magnetic mode frequency shift under a prolonged application of a continuous DC current for the input power (a) $P = 55$ mW and (b) 103 mW.

should remain at high temperature after the current was switched off and thus the resonance frequency should vary slowly after the power being switched off. But, f_r shows an immediate jump, and regains its the initial value as the sample cools down. It is safe to conclude from the data in Fig. 10 that any contribution due to sample is small compared to NLME effects.

The nature of strain mediated nonlinear ME effects in ferrite-ferroelectric composites was studied in detail and well understood. But there have been very few reports so far on NLME in spinel or hexagonal ferrites^{21–27}. We compare the strength of NLME in the spinel ferrite with similar reports for hexagonal ferrites. As mentioned earlier, the MSSW mode frequency tuning efficiency from Fig. 7 for the NZFO resonator $\Delta f_r/\Delta P \approx -4.1$ MHz/mW (or alternatively, $\Delta P/\Delta f_r = -0.25$ mW/MHz). In the case of M-type barium hexaferrite $\Delta f_r/\Delta P \approx +0.27$ MHz/mW²⁵. The efficiency was $+0.36$ MHz/mW for Al-substituted M-type strontium hexaferrite¹¹ and -14.2 MHz/mW for Y-type hexaferrite²⁶. Hence, the tuning efficiency for NZFO is higher than reported values for M-type hexaferrites, but not as high as for Y-type hexaferrite.

Conclusions

Evidence for electric field/current-induced NLME effects at room-temperature in single crystal nickel zinc ferrite resonator were obtained from studies on frequency tuning of MSSW modes at 8–20 GHz. It was found that the application of an in-plane DC current resulted in a down-shift in the MSSW mode frequencies that was linearly dependent on the DC electric power. This proportionality to P implies a nonlinear, quadratic in electric field E , nature of the observed ME effect and is similar to our earlier observations in M- and Y-type hexaferrites. The shift in mode frequencies due to NLME was independent of the mode frequency and was attributed to a reduction in the saturation magnetization of the ferrite. Using a rigorous theory for the MSSW modes in the ferrite slab with metal shielding, we were able to determine the variation of saturation magnetization with applied DC power. It was found that in all cases the magnetization decreased linearly with P at a rate of -2.50 G/mW. The

NLME related frequency tuning efficiency was 4.1 MHz/mW which is higher than the reported values for M-type hexaferrites with uniaxial anisotropy, but smaller than in Y-type hexaferrite with easy plane anisotropy. For the traditional *H*-tunable YIG filter the frequency tuning is linear with respect to the current in the solenoid coil and the tuning efficiency was 4–4.5 MHz/mW in the 10–18 GHz range³³. The results in this study indicate the utility of the NLME phenomenon in the spinel ferrite for planar, energy efficient electrically tunable microwave signal-processing devices that can be miniaturized and integrated with semiconductor devices.

Data availability

The datasets used and/or analyzed during the current study will be available from the corresponding author upon reasonable request.

Received: 6 July 2023; Accepted: 20 October 2023

Published online: 26 October 2023

References

- Zakharov, A., Rozenko, S., Litvintsev, S. & Ilchenko, M. Hairpin resonators in varactor-tuned microstrip bandpass filters. *IEEE Trans. Circuits Syst. II Exp. Briefs* **67**, 1874–1878 (2020).
- Poplavko, Y. M., Prokopenko, Y. V., Molchanov, V. I. & Dogan, A. Frequency-tunable microwave dielectric resonator. *IEEE Trans.* **49**, 1020–1026 (2001).
- Mansour, R. R., Huang, F., Fouladi, S., Yan, W. D. & Nasr, M. High-Q tunable filters: challenges and potential. *IEEE Microw. Mag.* **15**, 70–82 (2014).
- Adam, J. D. *An MSW tunable bandpass filter* 157–162 (Proc. IEEE Ultrason. Symp, 1985).
- Lebed, B. M. *et al.* Microwave devices based on magnetostatic surface waves propagated in thin magnetic films. *Microw. J.* **38**, 78–87 (1995).
- Manuilov, S. A., Fors, R., Khartsev, S. I. & Grishin, A. M. Submicron Y₃Fe₅O₁₂ film magnetostatic wave band pass filters. *J. Appl. Phys.* **105**, 033917 (2009).
- Zhang, Y. *et al.* Nonreciprocal isolating bandpass filter with enhanced isolation using metallized ferrite. *IEEE Trans. Microw. Theory Techn.* **68**, 5307–5316 (2020).
- Wu, J., Yang, X., Beguhn, S., Lou, J. & Sun, N. X. Nonreciprocal tunable low-loss bandpass filters with ultra-wideband isolation based on magnetostatic surface wave. *IEEE Trans. Microw. Theory Techn.* **60**, 3959–3968 (2012).
- Sun, N., Mingzhong, Wu, & Srinivasan, G. Ferrite-based multiferroic devices. *Mod. Ferrites Emerg. Technol. Appl.* **2**, 325–345 (2022).
- Liu, Y. *et al.* Magneto-electric interactions in composites of self-biased Y- and W-type hexagonal ferrites and lead zirconate titanate: Experiment and theory. *J. Appl. Phys.* **126**(11), 114102 (2019).
- Fetisov, L. Y., Chashin, D. V., Plekhanova, D. D., Saveliev, D. V. & Fetisov, Y. K. Electrical field control of magnetoelectric effect in composite structures with single crystal piezoelectrics. *J. Magn. Mater.* **470**, 93–96 (2019).
- Palneedi, H., Annapureddy, V., Priya, S. & Ryu, J. Status and perspectives of multiferroic magnetoelectric composite materials and applications. *Actuators* **5**(1), 9 (2016).
- Sun, N. *et al.* (eds) *Composite magnetolectrics: Materials, structures, and applications* (Elsevier, 2015).
- Vopson, M. M. Fundamentals of multiferroic materials and their possible applications. *Crit. Rev. Solid State Mater. Sci.* **40**(4), 223–250 (2015).
- Liu, J. & Nan, C. Decade of multiferroic researches. *Wuli* **43**(2), 88–98 (2014).
- Cheng, Y., Peng, B., Zhongqiang, Hu., Zhou, Z. & Liu, M. Recent development and status of magnetolectric materials and devices. *Phys. Lett. A* **382**(41), 3018–3025 (2018).
- Fetisov, Y. K. & Srinivasan, G. Electric field tuning characteristics of a ferrite-piezoelectric microwave resonator. *Appl. Phys. Lett.* **88**, 143503 (2006).
- Tatarenko, A. S., Gheevarghese, V. & Srinivasan, G. A magnetoelectric microwave band-pass filter. *Elec. Lett.* **42**, 540 (2006).
- Ciomaga, C. E. *et al.* Engineering magnetoelectric composites towards application as tunable microwave filters. *J. Phys. D Appl. Phys.* **49**(12), 125002 (2016).
- Chen, H. *et al.* Integrated tunable magnetoelectric RF inductors. *IEEE Trans. Microw. Theory Techn.* **68**(3), 951–963 (2020).
- Zavislyak, I. V., Popov, M. A. & Srinivasan, G. Current-induced nonlinear magnetoelectric effects in strontium hexaferrite. *Phys. Rev. B* **94**, 224419 (2016).
- Popov, M. A. & Zavislyak, I. V. Anisotropy of giant nonlinear magnetoelectric effects in hexaferrites with the magnetoplumbite structure. *Tech. Phys.* **63**, 1171–1176 (2018).
- Liu, Y. *et al.* Nonlinear magnetoelectric effects in Al-substituted strontium hexaferrite. *Sci. Rep.* **11**, 8733 (2021).
- Popov, M. *et al.* In-plane current induced nonlinear magnetoelectric effects in single crystal films of barium hexaferrite. *Sci. Rep.* **12**(1), 5374 (2022).
- Popov, M. A., Zavislyak, I. V. & Srinivasan, G. Current tunable barium hexaferrite millimeter wave resonator. *Microw. Opt. Technol. Lett.* **60**(2), 458–462 (2018).
- Popov, M. *et al.* Nonlinear magnetoelectric effects in Y-type hexaferrite microwave resonators. *J. Appl. Phys.* **128**(11), 113905 (2020).
- Popov, M. *et al.* Y-type hexagonal ferrite-based band-pass filter with dual magnetic and electric field tunability. *Sci. Rep.* **13**(1), 1179 (2023).
- Hellwege, K.-H. & Springer, A. M. *Landolt-Bornstein numerical data and functional relationships in science and technology, Group III Crystal and Solid State Physics, Vol 4 (b) Magnetic and Other Properties of Oxides* (Springer, 1970).
- Gurevich, A. G. & Melkov, G. A. *Magnetization oscillations and waves* (CRC, 1996).
- Yukawa, T., Takeda, S., Abe, K. & Ikenoue, J.-I. Dispersion surface of magnetostatic surface waves affected by perfect conductors. *IEEE Trans. Magn.* **MAG-16**, 687–689 (1980).
- Wu, J., Yang, X., Beguhn, S., Lou, J. & Sun, N. X. Nonreciprocal tunable low-loss bandpass filters with ultra-wideband isolation based on magnetostatic surface wave. *IEEE Trans. Microw. Theory Techn.* **60**(12), 3959–3968 (2012).
- Aubert, G. A novel approach of the magnetoelectric effects in ferrimagnets. *J. Appl. Phys.* **53**(11), 8125–8129 (1982).
- Harris, D. L. 4–40 GHz ferrite tuned filter. *Appl. Microw. Wirel.* **2**(4), 100–107 (1990).

Acknowledgements

The research at the Taras Shevchenko National University of Kyiv was supported by the Ministry of Education and Science of Ukraine, Project No. 0122U001908. The research at Oakland University was supported by grants from the National Science Foundation (ECCS-1923732, ECCS-EAGER-2236879, DMR-1808892) and the Air

Force Office of Scientific Research (AFOSR) Award No. FA9550-20-1-0114. The efforts at the University of Connecticut was supported by a grant from the National Science Foundation (ECCS-EAGER-2236879). The research at AFRL was partially supported by the AFOSR Award No. FA9550-23RXCOR001.

Author contributions

All authors contributed to this work. M.P., A.M., R.B., and S.S. involved in the magnetic characterization of the ferrite sample. M.P., J.I., H.Q., M.J., M.R.P and G.S. participated in the measurements of filter characteristics. M.J. and G.S. managed the grants that supported the research at University of Connecticut and Oakland University. All the authors contributed to the manuscript preparation.

Competing interests

The authors declare no competing interests.

Additional information

Supplementary Information The online version contains supplementary material available at <https://doi.org/10.1038/s41598-023-45530-4>.

Correspondence and requests for materials should be addressed to G.S.

Reprints and permissions information is available at www.nature.com/reprints.

Publisher's note Springer Nature remains neutral with regard to jurisdictional claims in published maps and institutional affiliations.



Open Access This article is licensed under a Creative Commons Attribution 4.0 International License, which permits use, sharing, adaptation, distribution and reproduction in any medium or format, as long as you give appropriate credit to the original author(s) and the source, provide a link to the Creative Commons licence, and indicate if changes were made. The images or other third party material in this article are included in the article's Creative Commons licence, unless indicated otherwise in a credit line to the material. If material is not included in the article's Creative Commons licence and your intended use is not permitted by statutory regulation or exceeds the permitted use, you will need to obtain permission directly from the copyright holder. To view a copy of this licence, visit <http://creativecommons.org/licenses/by/4.0/>.

© The Author(s) 2023